THE JOURNAL OF PHYSICAL CHEMISTRY C

Article

pubs.acs.org/JPCC

Evolution of 4e-Superatom Networks in $Au_4(AuL)_{1-12}$ Nanoclusters (L = Cl, SH, PH_2, SCH_3)

Zhimei Tian[†,‡] and Longjiu Cheng[*,†,§]

[†]Department of Chemistry, Anhui University, Hefei, Anhui 230601, China

[‡]School of Chemistry and Materials Engineering, Fuyang Teachers College, Fuyang, 236037, China

[§]AnHui Province Key Laboratory of Chemistry for Inorganic/Organic Hybrid Functionalized Materials, Hefei, Anhui 230601, China

Supporting Information

ABSTRACT: Ligand-protected gold (Au−L) nanoclusters have been widely studied due to their interesting optical, electronic, and charging properties. The superatom concept (SAC) and superatom-network (SAN) model are the two known tools, which are used to explain the electronic stability of Au−L nanoclusters. Ever since the crystal determination of the $Au_{102}(SR)_{44}$ cluster, there have been many subsequently crystallized Au−L nanoclusters. However, the size evolution of the superatom network in Au−L nanoclusters is still little known because of a lack of experimental data. To give a direct and overall view of size evolution of the superatom networks in Au−L clusters, the 4e $Au_4(AuL)_{1-12}$ (L = Cl, SH, PH_2, SCH_3) system is taken as a test case. The global minimum geometries have been explored using a first principle global minimization technique, namely, genetic algorithm from density functional theory geometry optimization (GA-DFT). The superatom networks in these structures are composed by two of the Au_3, Au_4, Au_5, or Au_6 2e-superatoms protected by staple motifs. The SAN model is used to explain the chemical bonding patterns, which are verified by chemical bonding analysis based on the adaptive natural density partitioning (AdNDP) method. The clusters which have triangular Au_3 and tetrahedral Au_4 superatoms are also analyzed by the recently proposed grand unified model. The aromatic analysis on the basis of nucleus-independent chemical shifts (NICS) method indicates that the superatoms in SANs of the clusters are highly aromatic. This work gives a clear size-evolution of the 4e-superatom networks for Au−L clusters with 1 to 12 ligands, which discovers the growth mechanism of Au−L clusters with different ligands.

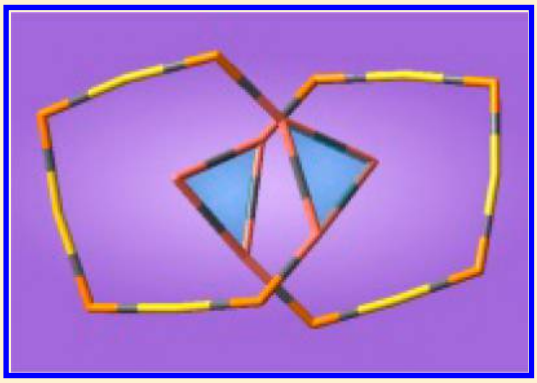

1. INTRODUCTION

Ligand-protected Au nanoclusters (Au−L) have attracted intensive research interest in recent years due to their unique electronic and geometrical structures, stability, and physical/chemical properties as well as potential applications in nanocatalysis, biomedicine and optical devices.[1−6] These unique properties of gold nanoclusters fundamentally result from the quantized electronic structure due to their size, and are different from those of larger counterparts, e.g., gold nanocrystals.[7] Significant advances have been achieved in experiments over the past few years in unveiling the geometric structures of gold nanoclusters. The first breakthrough is the crystal determination of $Au_{102}(SR)_{44}$ reported by the Kornberg group.[6] The $Au_{25}(SR)_{18}^-$ cluster is the second breakthrough, and the crystal structure has been reported separately by two groups almost at the same time.[4,8] Subsequently, the structures of $Au_{38}(SR)_{24}$,[9] $Au_{36}(SR)_{24}$,[10,11] $Au_{30}S(SR)_{18}$,[12,13] $Au_{28}(SR)_{20}$,[14] $Au_{24}(SR)_{20}$,[15] $Au_{23}(SR)_{16}^-$,[16] $Au_{20}(SR)_{16}$,[17] $Au_{18}(SR)_{14}$,[18,19] $Au_{133}(SR)_{52}$,[20] and $Au_{130}(SR)_{50}$,[21] were successfully determined by X-ray crystallography. On the theoretical size, theoretical prediction is a powerful tool to obtain the structures of Au−L nanoclusters. For example, the structures of $Au_{25}(SR)_{18}$[22−24] and $Au_{38}(SR)_{24}$[25−30] have been correctly predicted by several groups and confirmed by experiments. Structures of the experimentally synthesized Au−L nanoclusters can be well predicted by density functional theory (DFT) calculations and the success of DFT method in understanding and predicting the structures of Au-SR clusters are inspiring.[31−33] The experimental determination of $Au_{25}(SR)_{18}^-$ crystal structure proves the accuracy of theoretical predictions.[4,8,34]

To understand the intrinsic stability of Au−L nanoclusters, Häkkinen et al. proposed the superatom complex concept based on the jellium model.[35] Superatoms may be electronically stabilized by adsorption of ligands. The requirement for an electronically closed shell superatom complex, therefore, formulated as one determines the valence-electron count (V) of the $Au_m(SR)_n^q$ cluster (where q is the charge of the cluster) by $V = m - n - q$, and V is deduced from the superatomic number.[35] Each gold atom contributes one valence electron, and each SR or halogen group localizes one electron. The appropriate aufbau rule of super shells for spherical Au clusters is $|1S^2|1P^6|1D^{10}|2S^2 1F^{14}|2P^6 1G^{18}|\cdots$ (S−P−D−F−G−H− de-

Received: June 2, 2017
Revised: August 31, 2017
Published: August 31, 2017

DOI: 10.1021/acs.jpcc.7b05398
J. Phys. Chem. C 2017, 121, 20458−20467

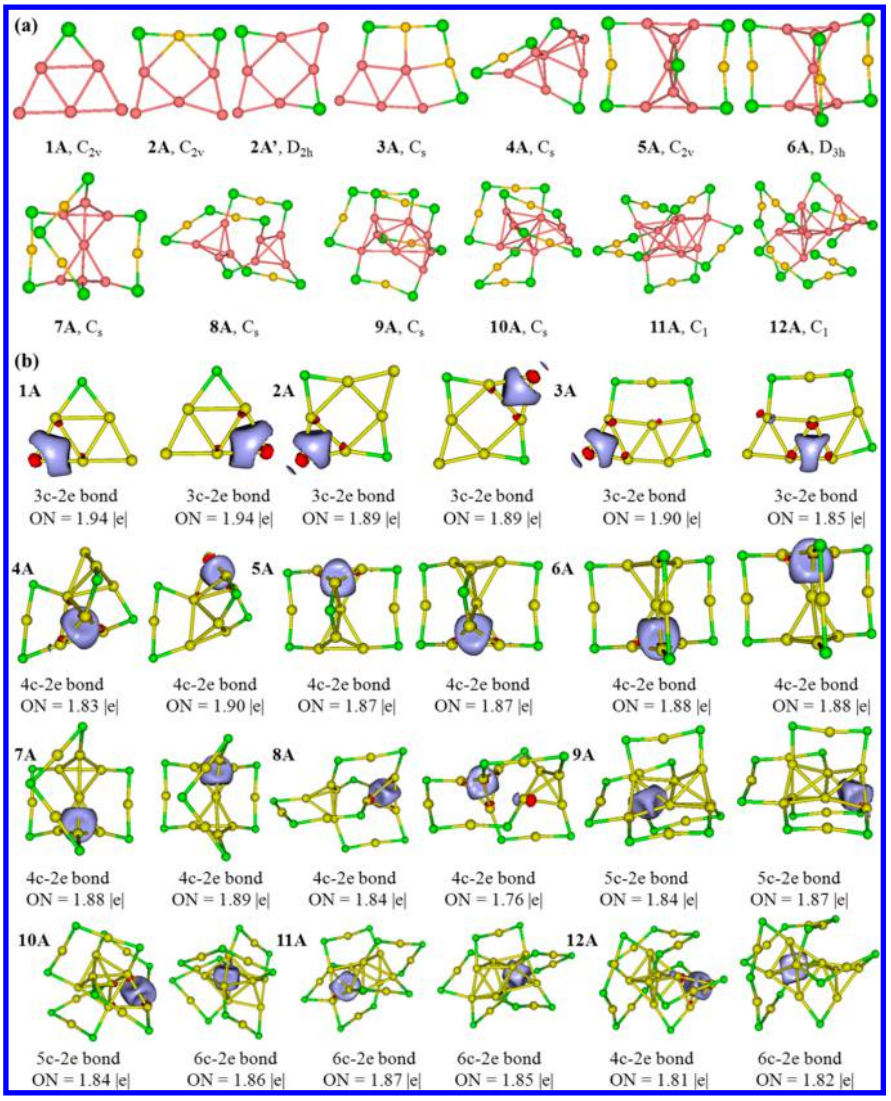

Figure 1. (a) Lowest-energy structures (**1A**−**12A**) of $Au_4(AuCl)_n$ (n = 1−12) clusters optimized at TPSS/def2-tzvp (Au) and 6-311G* (Cl) level of theory. Key: Au, yellow; Cl, green. The superatom networks of Au cores are shown in pink. (b) AdNDP natural bonding of the nc−2e delocalized superatomic orbitals in **1A**−**12A**.

note angular-momentum characters), associated with magic numbers 2, 8, 18, 34, 58, ... Exceptional stability is associated with a total count of 2, 8, 18, 34, 58, 92, 138, ... electrons, corresponding to strong electron shell closures. The superatom complex concept has achieved great success in predicting the stability of Au−L nanoclusters, which can be analyzed by the magic numbers. Jiang et al. proposed $[Au_{12}(SR)_9]^+$, $Au_8(SR)_6$, $Au_{10}(SR)_8$, and $Au_{15}(SR)_{13}$ clusters for the magic number 2.[36,37] $[Au_{25}(SR)_{18}]^-$ is associated with the magic number 8.[8] $[Au_{44}(SR)_{28}]^{2-}$ corresponds to the magic number 18.[38] $Au_{102}(SR)_{44}$ is associated with the magic number 58.[39,40]

For Au−L nanoclusters, $Au_{24}(SR)_{20}$, $Au_{20}(SR)_{16}$, and $Au_{18}(SR)_{14}$ as 4e clusters have been experimentally synthesized and characterized.[15,17−19] $Au_{24}(SR)_{20}$ features a bitetrahedral Au_8 kernel protected by four tetrameric staple-like motifs.[15] The structure of $Au_{20}(SR)_{16}$ features a vertex-sharing bitetrahedral Au_7 kernel and a $Au_8(SR)_8$ ring motif.[17] The large ring motif protects the Au_7 kernel through strong Au···Au bonding. Two groups separately synthesized the smallest crystallographically characterized gold cluster protected by thiolates, $Au_{18}(SR)_{14}$ cluster, almost at the same time.[18,19] The structure of $Au_{18}(SR)_{14}$ cluster exhibits a bioctahedral Au_9 kernel protected by staple-like motifs including one tetramer, one dimer, and three monomers. This Au_9 core is built by two octahedral Au_6 cores sharing one triangular face.[19] $Au_{24}(SR)_{20}$, $Au_{20}(SR)_{16}$, and $Au_{18}(SR)_{14}$ nanoclusters form the 4e nanocluster family, with kernels ranging from Au_8^{4+} to Au_7^{3+} and to Au_9^{5+} with decreasing size.

Cheng and Yang proposed the superatom-network (SAN) model to explain the electronic stability of nonspherical shells of metal clusters.[41] The electronic stability of the 4e $Au_{18}(SR)_{14}$, $Au_{20}(SR)_{16}$, and $Au_{24}(SR)_{20}$ nanoclusters follow the SAN model, and Au_8^{4+} cores of the three clusters could be viewed as a network of two Au_4 superatoms.[41] Recently, the Au_9^{5+} core of the experimentally synthesized $Au_{18}(SR)_{14}$ can be viewed as a unique combination of two fused octahedral Au_6 superatom units according to the SAN model.[19] The Au-core in $Au_{12}Cl_8$ cluster can be viewed as Au_4 SAN as well.[42] The "divide-and-protect" approach was originally proposed by Häkkinen et al.,[25] which has been widely used to predict $Au_m(SR)_n$ clusters.[4,29,43−45] On the basis of the approach,

DOI: 10.1021/acs.jpcc.7b05398
J. Phys. Chem. C 2017, 121, 20458−20467

$Au_m(SR)_n$ clusters can be viewed as Au cores protected by protecting motifs.

Recently, a grand unified model (GUM) has been proposed by Zeng et al., which can offer a universal description of the structures of diverse liganded gold clusters.[46] According to GUM, gold atoms on surface of the gold core can be assigned to three valence states which are in names of three flavors: i.e., bottom (1e), middle (0.5e), and top (0e) flavor. The triangular elementary block Au_3 (2e) and tetrahedral elementary block Au_4 (2e) are identified to describe the stabilities of 71 ligand-protected gold clusters reported in literature experimentally and theoretically; namely, the gold cores in the clusters can be viewed as packing of Au_3 (2e) and Au_4 (2e) elementary blocks.

There are many major progresses in resolving the structures of Au−L clusters, however, to the best of our knowledge, size evolution of superatom networks in ligand-protected gold clusters is still little known because lack of experimental data. For 4e Au−L nanoclusters, only three clusters have been synthesized.[15,17−19] It is necessary for us to predict 4e clusters and find the growth patterns of them, which may provide a certain reference to the synthesis of 4e-superatomic Au−L clusters in future experiments. In this work, we report a systematic study of low-lying structures of 4e-superatomic ligand-protected Au nanoclusters: $Au_4(AuL)_{1-12}$ (L = Cl, SH, PH_2, SCH_3), which is a continuous work of our previous work.[47] Major attention is placed on the search for structures of the lowest energy clusters of $Au_4(AuL)_{1-12}$. The structures of $Au_4(AuL)_{1-12}$ nanoclusters with four different ligands are given, and the size evolution of the 4e-superatom Au cores' networks based on the "divide-and-protect" approach and SAN model can be seen clearly. The size evolution of the 4e superatom complex is useful in predicting the structures of Au−L nanoclusters with a count number of 4 and understanding the evolution of superatom networks.

2. COMPUTATIONAL METHODS

The global minimum search for the isomers of $Au_4(AuL)_{1-12}$ (L = Cl, SH, PH_2, SCH_3) clusters is performed using a genetic algorithm (GA) coupled with DFT, which has been successfully applied in the structural prediction of a number of systems.[48−54] GA is a search heuristic that mimics the process of natural selection.[55] This heuristic is routinely used to generate useful solutions to optimization and search problems. GA belongs to the larger class of evolutionary algorithms, which generate solutions to optimization problems using techniques inspired by natural evolution.[56,57] The quantum chemical calculations are carried out on the Gaussian 09 suite of programs.[58] In the optimization procedure, the def2-tzvp basis set is used for Au which obtains from the basis set exchange,[59,60] and 6-311G* basis set is used for Cl, S, P, C and H with generalized gradient approximation method by Tao−Perdew−Staroverov−Scuseria (GGA-TPSS)[61] without any symmetry constraint. The normal-mode frequencies are also computed at the same level to ensure that they belong to real minima. The natural bond orbital (NBO)[62] analyses are calculated using the TPSS functional with a Lanl2dz basis set for Au and a 6-31G* basis set for Cl, S, P, C, and H. To elucidate the nature of the chemical bonding, the adaptive natural density partitioning (AdNDP) is used to analyze the chemical bonding.[63] The AdNDP method is widely used to analyze the chemical bondings in boron clusters,[63−65] Au clusters[66,67] and $Au_m(SR)_n$ nanoclusters.[68,69] Molecular visualization is performed using MOLEKEL 5.4.[70]

3. RESULTS AND DISCUSSIONS

The lowest-lying equilibrium geometries and their symmetries of $Au_4(AuL)_{1-12}$ and the AdNDP natural bonding of the *n*c−2e delocalized superatomic orbitals of them are shown in Figures 1−3. The color of Au cores for each structure is emphasized in pink in order to see it more clearly. We locate the global minimum (GM) structures and some relative stable isomers of $Au_4(AuL)_{1-12}$ (L = Cl, SH, PH_2) indexed as Roman numerals (such as **I**, **II**, **III**, ... for $Au_4(AuCl)_{1-12}$ by energy from low to high) in Figures S1−S3, respectively. Chemical bonding analysis is performed using the AdNDP method to confirm the superatom networks in clusters.

3.A. Geometric and Electronic Structures. *$Au_4(AuCl)_{1-12}$*.

Geometries of the GMs of $Au_4(AuCl)_{1-12}$ clusters are given in Figure 1a, and the corresponding AdNDP natural bonding orbitals of the *n*c−2e delocalized superatomic orbitals are given in Figure 1b. When n = 1−3, Au_4−AuCl, $Au_4(AuCl)_2$, and $Au_4(AuCl)_3$ clusters consist of a SAN of two Au_3 superatoms protected by −Cl, −Cl−Au−Cl− (monomer) and −Cl−Au−Cl−Au−Cl− (dimer), respectively. On the basis of GUM, each Au_5 core in 1A-3A consists of two triangular Au_3 blocks. **2A′** is also the GM of n = 2, which consists of a SAN of two nonconjugate Au_3 superatoms (Au_3 blocks) protected by -Cl units. There are isolated Au atoms in the SANs of **1A**, **2A**, **2A′**, and **3A**, which disagree with the "divide-and-protect" model. AdNDP analysis in Figure 1b reveals two 3-center 2-electron (3c−2e) bonds in **1A-3A** with occupancy numbers (ON) = 1.85−1.94 |e|. Such an Au_3 2e-superatom has not been viewed in experimentally produced Au-SR clusters, however, it has been revealed in theoretically predicted $Au_{15}Cl_5$ and Au_2-$(AuCl)_n$ (n = 1−4) clusters.[42,47] When n = 4−7, the clusters consist of two vertex-sharing tetrahedral Au_4 superatoms/blocks protected by three motifs, and such a vertex-sharing Au_7 kernel is consistent with that in the experimentally determined structure of 4e cluster $Au_{20}(SR)_{16}$.[17] Note that the multicenter bonding concept was previously used, and a four-atomic tetrahedron with a 4c−2e bond inside was used as a building block to design new 3D clusters.[71] **8A** is composed of two nonconjugate tetrahedral Au_4 superatoms/blocks protecting by one −Cl, two monomers, and one dimer. AdNDP analysis reveals the two 4c−2e bonds in **4A-8A** with ONs = 1.76−1.90 |e|. **4A−8A** follow the "divide-and-protect" model and GUM very well. The tetrahedral Au_4 core has been theoretically predicted in small nanoparticles, such as in $Au_{10}(SR)_8$ and $Au_8(SR)_6$ clusters.[36,37] The Au-core of **9A** is a SAN of two edge-sharing trigonal bipyramid Au_5 superatoms, which is protected by three monomers and one dimer. AdNDP analysis reveals two 5c−2e bonds in **9A** with ONs = 1.84 and 1.87 |e|, respectively. **10A** can be viewed as a SAN of one rectangular pyramid Au_5 and one octahedronal Au_6 superatom stapled by two monomer and two dimer units. The ONs of 5c−2e and 6c−2e bonds in **10A** are 1.86 and 1.84 |e|, respectively. The bipyramid and rectangular pyramid Au_5 superatoms have been predicted in $Au_{11}Cl_9$ cluster.[42] **11A** is composed of two octahedronal Au_6 superatoms with triangular-face-sharing stapled by four monomers and one dimer units. ONs of the 6c−2e bonds are 1.87 and 1.85 |e|, respectively. Worth noting is that the regularity of two motifs connects to two nearest vertices of Au cores is broken in **9A** and **11A**. Namely, each of the Au_5 and Au_6 superatoms in **9A** and **11A** has one Au atom overprotected, respectively. **12A** is a broken structure with two bare −Cl, which is composed of a SAN of

DOI: 10.1021/acs.jpcc.7b05398
J. Phys. Chem. C 2017, 121, 20458−20467

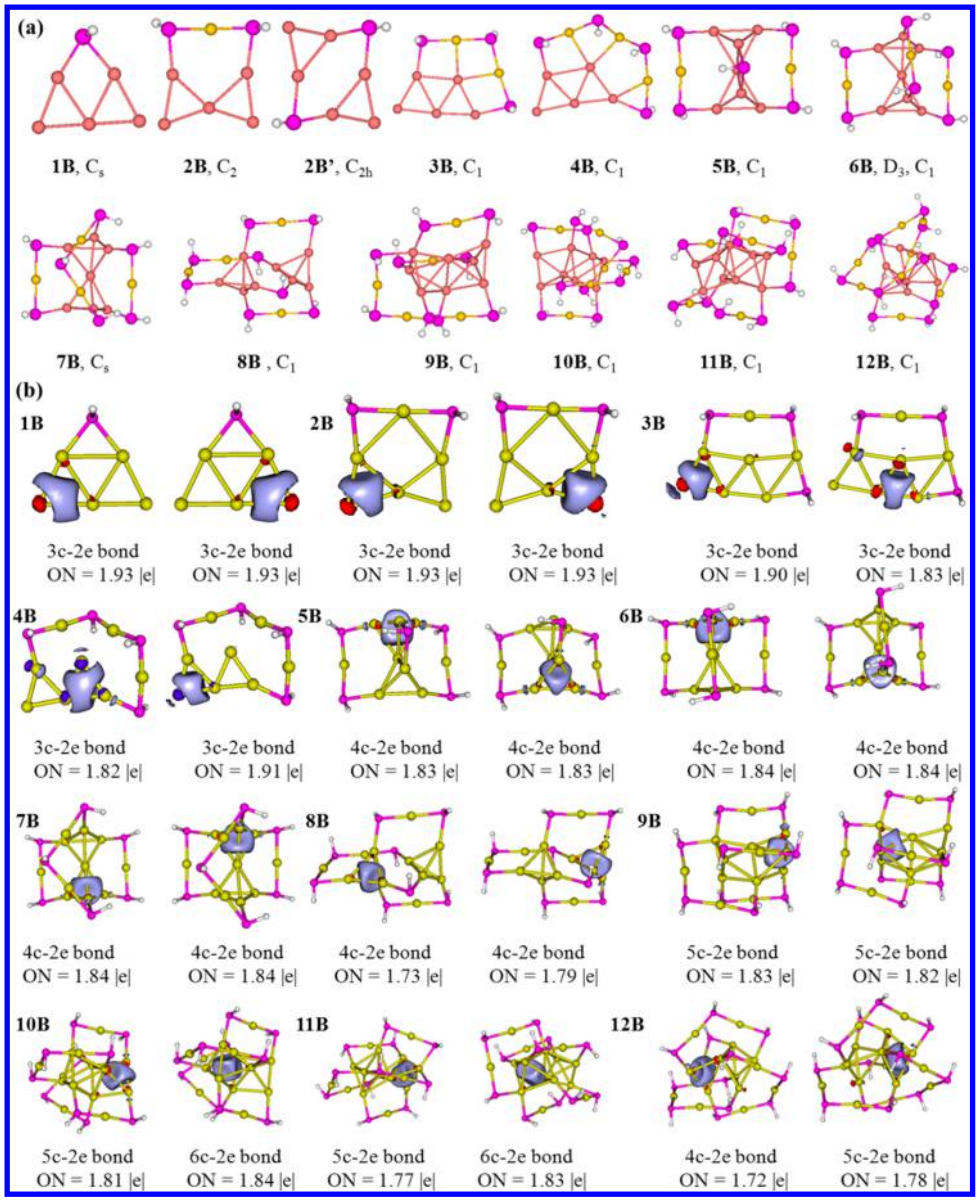

Figure 2. (a) Lowest-energy structures (**1B**−**12B**) of $Au_4(AuSH)_n$ (n = 1−12) clusters optimized at TPSS/def2-tzvp (Au) and 6-311G* (S, H) level of theory. Key: Au, yellow; S, purple; H, white. The superatom networks of Au cores are shown in pink. (b) AdNDP natural bonding of the nc−2e delocalized superatomic orbitals in **1B**−**12B**.

one vertex-sharing Au_4 and one octahedronal Au_6 superatoms protected by one −Cl, one monomer, one dimer, and one trimeric $-Cl-(AuCl)_3$- unit. On the basis of AdNDP analysis, the ONs of 4c−2e and 6c−2e bonds in **12A** are 1.82 and 1.81 |el, respectively. The octahedronal Au_6 superatoms in 10A-12A has been revealed in the DFT predicted $Au_{12}(SR)_9^+$ cluster.[37] Jiang et al. predicted theoretically that small halide ligands, such as Cl, may have similar behavior as thiolate, i.e., linear Cl−Au−Cl vs RS−Au−SR.[72] The conformation of interlocked staple motifs surrounding gold kernels in 9A-12A resembles the condition in 4e $Au_{22}(SR)_{18}$ and $Au_{24}(SR)_{20}$ clusters.[73,74] Noteworthy is that $-Cl-(AuCl)_n-$ motif has been viewed in the experimentally synthesized chloride-rich $Au_{36}(SCH_2Ph-^tBu)_8Cl_{20}$ cluster.[75] A linear pentameric SR−Au−Cl−Au−Cl−Au−Cl−Au−Cl−Au−Cl motif and Cl are observed in the cluster. Moreover, it is the first time to observe "Au−Cl−Au" staple motif in thiolate protected gold clusters. For comparison, the longest staple motif in $Au_4(AuCl)_{1-12}$ clusters present in 12A which has one trimeric $-Cl-(AuCl)_3-$ staple motif. The Cl−Au−Cl staple motifs in $Au_4(AuCl)_{1-12}$ clusters are almost linear.

$Au_4(AuSH)_{1-12}$. Geometries of the GMs of $Au_4(AuSH)_{1-12}$ clusters are given in Figure 2a, and the corresponding AdNDP natural bonding orbitals of nc−2e delocalized superatomic orbitals are given in Figure 2b. When n = 1−3, the frameworks are identical to those of **1A**−**3A**, and the Au cores are 2 × 2e SANs of two Au_3 superatoms. The Au_3 superatoms are two Au_3 blocks based on GUM. **4B** consists of a SAN of two vertex-sharing Au_3 superatoms/blocks protected by a trimeric staple motif. Obviously, **1B**−**4B** do not follow the "divide-and-protect" model, which depends on Au···Au contacts in the clusters to obtain their stability. AdNDP analysis reveals two 3c−2e bonds in **1B**−**4B** with ONs = 1.82−1.93 |el. When n = 5−8, the frameworks are identical to those of **5A**−**8A**, and the Au cores are SANs (2 × 2e) of two Au_4 superatoms/blocks. AdNDP analysis in Figure 2b confirms the Au_4 superatoms in

DOI: 10.1021/acs.jpcc.7b05398
J. Phys. Chem. C 2017, 121, 20458−20467

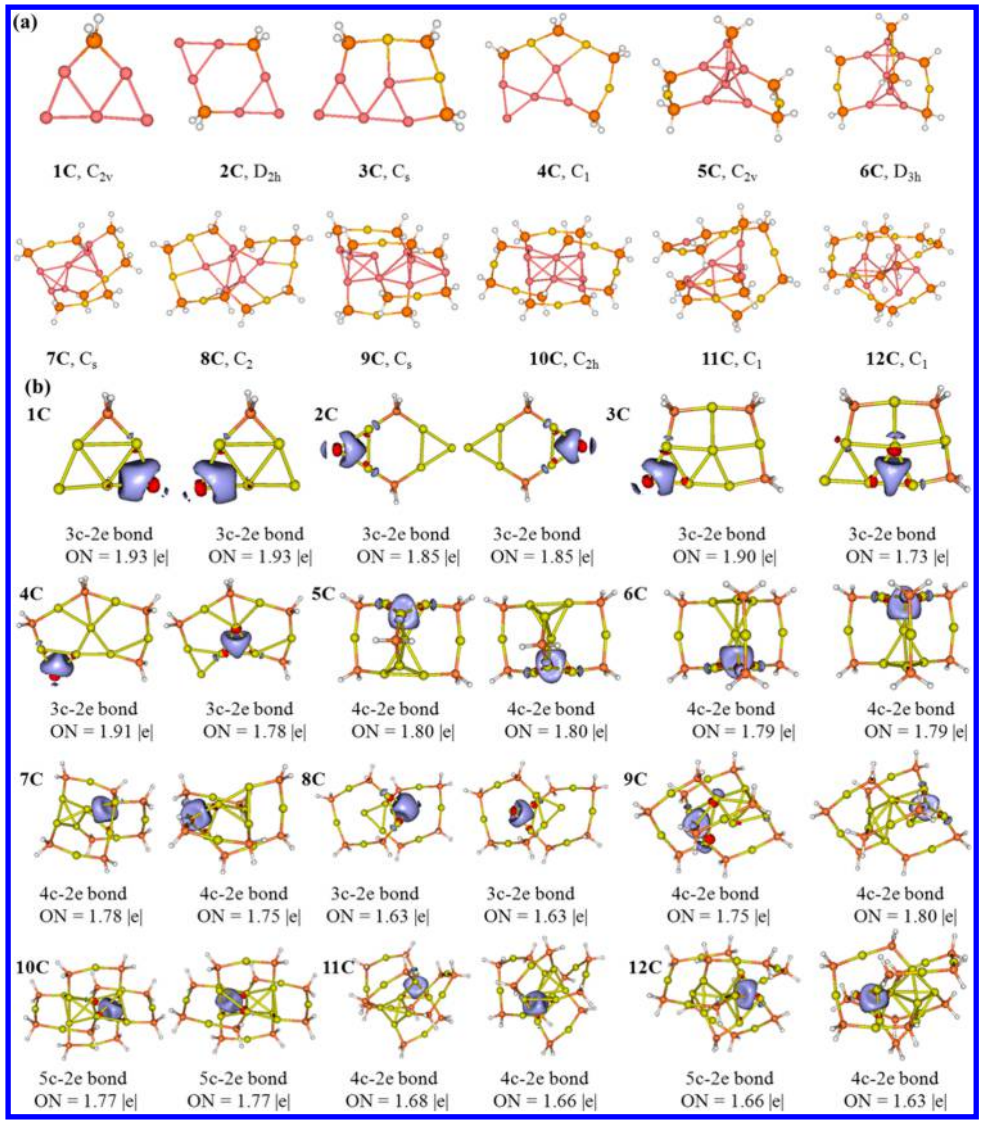

Figure 3. (a) Lowest-energy structures (**1C**−**12C**) of $Au_4(AuPH_2)_n$ (n = 1−12) clusters optimized at TPSS/def2-tzvp (Au) and 6-311G* (P, H) level of theory. Key: Au, yellow; P, orange; H, white. The superatom networks of Au cores are shown in pink. (b) AdNDP natural bonding of the nc−2e delocalized superatomic orbitals in **1C**−**12C**.

5B−**8B**. **5B**−**8B** follow "divide-and-protect" model very well. The frameworks of **9B** and **10B** are identical to those of **9A** and **10A**, respectively. Worth noting is that there is one over-protected Au atom in one of the Au_5 cores of **9B**. AdNDP analysis reveals two 5c−2e bonds in **9B** with ONs = 1.82 and 1.83 |e|, respectively. The ONs of Au_5 and Au_6 superatoms in **10B** are 1.81 and 1.84 |e|, respectively. **11B** consists of a SAN (2 × 2e) of edge-sharing Au_5 and Au_6 superatoms stapled by four monomers and one dimer units, and one Au atom in Au_6 superatom is overprotected. The ONs of Au_5 and Au_6 superatoms in **11B** are 1.84 and 1.77 |e|, respectively. **12B** is composed of a SAN of one vertex-sharing Au_4 and one trigonal bipyramid Au_5 superatoms, protected by one −SH, one dimer and one trimer units. AdNDP analysis reveals that the ONs of Au_4 and Au_5 superatoms in **12B** are 1.72 and 1.78 |e|, respectively.

$Au_4(AuPH_2)_{1-12}$. Geometries of the GMs of $Au_4(AuPH_2)_{1-12}$ clusters are given in Figure 3a, and the corresponding AdNDP natural bonding orbitals of the nc−2e delocalized superatomic orbitals are given in Figure 3b. Same to L = Cl, SH, the Au cores of L = PH_2 are SANs (2 × 2e) of two Au_3 superatoms when n = 1−3, and SANs of two Au_4 superatoms when n = 5−7. The Au_6 cores in 5C-7C are similar. Taking the Au_6 core in 5C as an example, it is composed of two tetrahedral Au_4 blocks, fused together by sharing an Au atom. The latter contributes 0.5e valence electron to the Au_4 block. Other six vertex Au atoms are bonded with the PH_2 group and each contributes 0.5e valence electron to the Au_4 block. Each of the four Au atoms in the Au_4 block has the middle flavor. The ONs of the superatoms in **1C**−**7C** are in the range of 1.75−1.93 |e|. The framework of **4C** is identical to that of **4B**, however, they are different from that of **4A**. The framework of **8C** is seriously different from those of **8A** and **8B**. **8C** is a very interesting structure in C_2 symmetry, which consists of a 2 × 2e SAN of two Au_3 superatoms protected by two trimers and the isolated Au atoms in the Au core are stabilized by Au···Au contacts. According to the GUM, the Au_6 core of **8C** is composed of two triangular Au_3 blocks. Four Au atoms of the Au_6 core are bonded with ligands and thus have 1e valence electron or bottom flavor. Each of the two isolated Au atoms contributes 0e valence electron and has top flavor. Clearly, the number of valence electrons in Au_3 blocks satisfies the duet rule.[46] As a

DOI: 10.1021/acs.jpcc.7b05398
J. Phys. Chem. C 2017, 121, 20458−20467

consequence, higher thermal stability is expected. The ONs of the Au_3 superatoms in **8C** are relatively small (1.63 lel) compared to those in **1C**−**4C**. It is concluded that Au···Au contacts affect the ONs in **8C**. The framework of **9C** is different from those of **9A** and **9B** in that the Au cores of **9C** is a SAN of two vertex-sharing Au_5 superatoms whereas those of **9A** and **9B** are edge-sharing Au_5 superatoms. AdNDP analysis reveals two 5c−2e bonds in **9C** with ONs = 1.75 and 1.80 lel, respectively. **10C** is different from **10A** and **10B**, which is in C_{2h} symmetry and consists of a SAN of two edge-sharing Au_5 superatoms stapled by two monomer and two dimer staple motifs, and the ONs are both 1.77 lel. **11C** is different from **11A** and **11B**, which is composed of a SAN (2 × 2e) of two vertex-sharing Au_4 superatoms protected by two monomers and a very long staple motif $-PH_2-(AuPH_2)_6-$. Chemical bonding analysis given by AdNDP reveals two conjugated 4c−2e bonds with ONs = 1.66 and 1.68 lel, respectively (Figure 3b). The framework of **12C** is identical to that of **12B** discussed above. Chemical bonding analysis reveals that the ONs of the 4c−2e and 5c−2e bonds in **12C** are 1.63 and 1.65 lel, respectively.

Generally, $-PR_2$ ligand protected gold clusters through top site or bridge site. For example, PPh_3 groups in $[Au_{14}(PPh_3)_8(NO_3)_4]$ and $[Au_{25}(PPh_3)_{10}(SC_nH_{2n}1)_5Cl_2]_2$ protect gold cores via top site.[76,77] However, similar to $Au_4(AuCl)_{1-12}$ and $Au_4(AuSH)_{1-12}$, staple motifs like $-PH_2-Au-PH_2-$, $-PH_2-Au-PH_2-Au-PH_2-$ present in $Au_4(AuPH_2)_{1-12}$ clusters. Gold atoms interact with PR_2 groups to form staple like units in $Au_4(AuPH_2)_n$ clusters, which is similar to the homoleptic $[Au(PR_2)]_n$ clusters. The -$[Au\text{-}PR_2]_n$- rings present in the synthesized cyclic oligomers of $[Au(PR_2)]_n$ (n = 3, 4, 6) clusters.[78−80] A ring structure of $Au_8(PR_2)_8$ is revealed in the structure of the synthesized tetrameric $[Au(MesP(CH_2)_3PMes)Au]_4$.[81]

$Au_4(AuSCH_3)_{1-12}$. For comparison, we also calculate the structures of $Au_4(AuSCH_3)_{1-12}$ clusters to see how $-SCH_3$ and −SH ligands affect the structures of the 4e clusters. The global minima of $Au_4(AuSCH_3)_{1-12}$ clusters are given in Figure 4. Compared to the structures in Figure 2, it is evident that the structural frameworks of $Au_4(AuSCH_3)_{1-12}$ clusters are absolutely identical to those of $Au_4(AuSH)_{1-12}$ clusters. In other words, when we replace the −SH ligand in $Au_4(AuSH)_{1-12}$ by $-SCH_3$, the frameworks do not change. Ligand effects between SH and SCH_3 are not obvious, which reminds us that we can use SH instead of SCH_3 to predict the structures of $Au_4(AuSCH_3)_n$ to save computational cost. The Au_5 kernels in **1D**−**4D** are built on two vertex-sharing Au_3 superatoms. The Au_5 kernel in **2D′** is composed of two nonconjugate Au_3 supertoms. Worth noting is that the Au_5 kernel has not been viewed in the experimentally produced Au−L clusters. The Au_7^{3+} kernels in **5D**, **6D**, and **7D** have been viewed in the experimentally synthesized $Au_{20}(SR)_{16}$ cluster, which are all vertex-sharing Au_4 conformations.[17] The Au_8^{4+} kernel with two 2e tetrahedral superatoms in **8D** has been viewed in the experimentally synthesized $Au_{24}(SR)_{20}$ cluster.[15] The Au_9^{5+} kernel in **11D** is different from that in the experimentally synthesized $Au_{24}(SR)_{20}$ cluster, which is built by one Au_5 and one Au_6 superatoms sharing one edge. The kernels in **9D**, **10D**, and **12D** are all Au_8^{4+}; however, they are different from each other, as they consist of two edge-sharing Au_5 superatoms, edge-sharing Au_5 and Au_6 superatoms, and vertex-sharing Au_5 and Au_6 superatoms, respectively.

The structural evolutions of the Au cores with increasing number of AuL in $Au_4(AuL)_n$ clusters are presented. For **1A**−**3A**, **1B**−**4B**, **1C**−**4C**, and **1D**−**4D**, the Au cores are composed of two Au_3 triangular superatoms/blocks. The Au cores consist of two tetrahedral Au_4 superatoms/blocks for **4A**−**8A**, **5B**−**8B**, **5C**−**7C**, and **5D**−**8D**. When n > 8, the Au cores are composed of Au_4, Au_5, or Au_6 superatoms. The size evolution of Au cores can be understood by superatoms and blocks. The size of the Au cores evolves from Au_6^{2+} to Au_7^{3+}, to Au_8^{4+}, and finally to Au_8^{4+}, Au_9^{5+} as cluster size increases.

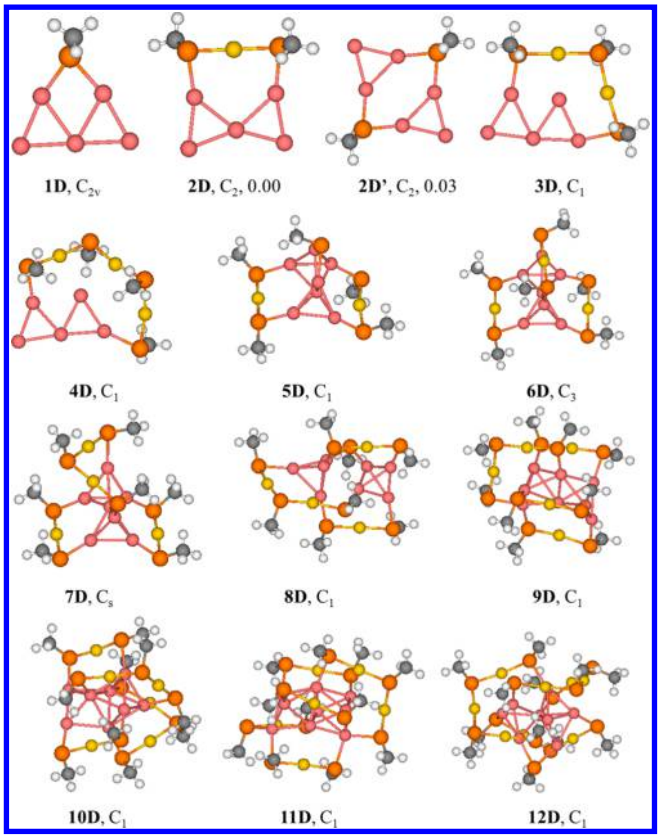

Figure 4. Lowest-energy structures (**1D**−**12D**) of $Au_4(AuSCH_3)_n$ (n = 1−12) clusters optimized at TPSS/def2-tzvp (Au) and 6-311G* (S, C, H) level of theory. Key: Au, yellow; S, orange; C, black; H, white. The superatom networks of Au cores are shown in pink. Also given is the energy gap of **2D** and **2D′**.

When the cluster size $n \leq 4$ (except $Au_4(AuCl)_4$), the frameworks of the clusters are planar or quasiplanar. The clusters follow SAN model, however, they do not follow the "divide-and protect" model, in which the Au···Au contact plays an important role in stabilizing the clusters. The framework of the GMs of the clusters changes from planar or quasiplanar to three-dimensional as n increases. When n > 4, the clusters follow SAN model and "divide-and-protect" model well with exception being Au atoms in Au cores overprotected in several structures. Ligand effects are also evident for the $Au_4(AuL)_{1-12}$ clusters. When n = 1−4, the clusters resemble each other when n = 1−3 and 5−7 for the four ligands. The structure of $Au_4(AuCl)_4$ is distinctively different from those of $Au_4(AuSH)_4$ and $Au_4(AuPH_2)_4$, which may be due to the strong polarity of Au−Cl bond. $Au_4(AuPH_2)_8$ cluster is different from corresponding $Au_4(AuCl)_8$ and $Au_4(AuSH)_8$ clusters, and the reason may be that Au−P polarity is weaker compared to Au−Cl and Au−S. The framework of the clusters for L = PH_2 are different from those for L = Cl and SH when n = 9−11. For L = Cl and PH_2, the frameworks resemble each other when n = 1−3 and 5−10. Particularly, the cluster is broken at n = 12 for L = Cl

DOI: 10.1021/acs.jpcc.7b05398
J. Phys. Chem. C 2017, 121, 20458−20467

Table 1. NICS(0) Values (ppm) of the Superatoms in 1A-12A, 1B-12B and 1C-12C clusters

system	type	NICS(0)/ppm	system	type	NICS(0)/ppm	system	type	NICS(0)/ppm
1A	3c−2e	−29.6	**1B**	3c−2e	−27.4	**1C**	3c−2e	−24.1
	3c−2e	−29.6		3c−2e	−27.4		3c−2e	−24.1
2A	3c−2e	−37.8	**2B**	3c−2e	−31.0	**2C**	3c−2e	−25.3
	3c−2e	−37.8		3c−2e	−31.1		3c−2e	−25.3
3A	3c−2e	−29.8	**3B**	3c−2e	−28.0	**3C**	3c−2e	−27.7
	3c−2e	−29.0		3c−2e	−26.5		3c−2e	−25.4
4A	4c−2e	−29.7	**4B**	3c−2e	−27.6	**4C**	3c−2e	−27.5
	4c−2e	−27.3		3c−2e	−26.9		3c−2e	−29.0
5A	4c−2e	−33.5	**5B**	4c−2e	−28.9	**5C**	4c−2e	−22.8
	4c−2e	−33.5		4c−2e	−28.9		4c−2e	−22.9
6A	4c−2e	−38.3	**6B**	4c−2e	−33.1	**6C**	4c−2e	−26.8
	4c−2e	−38.3		4c−2e	−33.2		4c−2e	−26.8
7A	4c−2e	−38.1	**7B**	4c−2e	−33.3	**7C**	4c−2e	−25.2
	4c−2e	−38.1		4c−2e	−33.4		4c−2e	−25.7
8A	4c−2e	−37.1	**8B**	4c−2e	−33.4	**8C**	3c−2e	−28.6
	4c−2e	−38.1		4c−2e	−33.1		3c−2e	−28.6
9A	5c−2e	−33.1	**9B**	5c−2e	−27.9	**9C**	5c−2e	−34.0
	5c−2e	−36.5		5c−2e	−26.3		5c−2e	−23.5
10A	5c−2e	−24.2	**10B**	5c−2e	−21.5	**10C**	5c−2e	−22.2
	5c−2e	−24.3		6c−2e	−22.7		5c−2e	−22.2
11A	6c−2e	−32.3	**11B**	4c−2e	−23.5	**11C**	4c−2e	−24.8
	6c−2e	−24.1		6c−2e	−21.6		4c−2e	−26.0
12A	4c−2e	−30.7	**12B**	4c−2e	−25.8	**12C**	4c−2e	−14.3
	6c−2e	−23.9		5c−2e	−19.9		5c−2e	−25.4

perhaps due to the strong Au−Cl polarity which has also found in $(AuCl)_n$ clusters.[82] In the protecting staple motif size, the length of staple motifs for L = Cl and SH is short with the longest staple motif being trimer, whereas that for L = PH_2 could be very long, and the staple motif of $Au_4(AuPH_2)_{11}$ is $-PH_2-(AuPH_2)_6-$. The experimentally viewed Au kernels such as Au_7^{3+}, Au_8^{4+} and Au_9^{5+} have been revealed in the studied system.

3.B. Aromaticity. The nucleus-independent chemical shifts (NICS) method was proposed as an aromaticity/antiaromaticity criterion,[83] which uses the absolute magnetic shieldings as a magnetic index of aromaticity. NICS value is the most widely used quantitative measure for aromaticity. Negative NICS values mean aromaticity, whereas positive NICS values mean antiaromaticity. NICS is an effective aromaticity criterion, which has been successfully used to predict the aromaticity of aromahydrocardons,[83] boron clusters, fullerenes,[84] and all-metal compounds,[85] etc. In 2001, Boldyrev and Wang et al. reported the experimental and theoretical evidence of aromaticity in Al_4^{2-}, an all-metal compound.[86] The NICS values at the centers (coined as NICS(0)) are better suited for evaluation of the aromaticity for all-metal species.[87] The NICS(0) values of the superatoms in $Au_4(AuCl)_n$, $Au_4(AuSH)_n$, and $Au_4(AuPH_2)_n$ clusters are calculated with TPSS/lanl2dz and 6-31G* methods through the gauge-including atomic orbital (GIAO) method[88] implemented in Gaussian 09. Table 1 shows NICS(0) values of the superatoms in the clusters, and also shown are the concrete *n*c−2e (*n* = 3, 4, 5 or 6) superatom types. From the table, we can see that the NICS(0) values are largely negative, which indicate that the superatoms are highly aromatic due to delocalization of the *n*c−2e bonds. In addition, the aromaticity of 4c−2e bond is bigger than those of 3c−2e, 5c−2e, and 6c−2e bonds. When we compare the NICS(0) values of 3c−2e bonds in **8C** to the corresponding 4c−2e bonds in **8A** and **8B**, we can clearly obtain that the aromaticity of 3c−2e bonds in **8C** are weaker than those of 4c−2e bonds. From the geometric analysis, we can see that the Au···Au contacts in **8C** are stronger than those in **8A** and **8B**, thus we infer that Au···Au contacts may affect the aromaticity of the superatoms. Namely, the stronger the Au···Au contacts, the weaker the aromaticity of the superatoms is.

3.C. Stability. To investigate the stability of the clusters, the atomization energies ($E_{at} = (n + 4)E_{Au} + E_L - E_{Au_4(AuL)_n}$) and the average energies (a four-parameter fitting of the GMs: $E_{ave} = a + b \times n^{1/3} + c \times n^{2/3} + d \times n$) of the clusters are calculated. The energies ($E_{at} - E_{ave}$) of the GMs as a function of the cluster size (n) are depicted in Figure 5, where upward peaks represent the clusters are more stable and downward peaks represent the clusters are less stable. Figure 5 shows upward peaks at n = 2, 6, and 11, indicating that $Au_4(AuL)_2$, $Au_4(AuL)_6$, and $Au_4(AuL)_{11}$ (L = Cl, SH, and PH_2) clusters are more stable compared to neighboring clusters. From the figure, we also obtain that at n = 8, the cluster is particularly stable for L = PH_2 compared to L = Cl and SH. And the reason may be that **8C** has a distinctively different structure from those of **8A** and **8B**. There are more Au···Au contacts in **8C** than those in **8A** and **8B**. Worth noting is that $Au_4(AuL)_6$ clusters are the most stable clusters for the three ligands. It is concluded that $Au_4(AuL)_6$ (L = Cl, SH and PH_2) clusters may be synthesized in future.

4. CONCLUSIONS

In present work, the superatomic structures of $Au_4(AuL)_{1-12}$ (L = Cl, SH, PH_2, SCH_3) clusters have been studied, all of which have four free valence electrons in gold cores. The GMs of the clusters are investigated using a combination of GA and DFT methods with the TPSS functional. The "divide-and-protect" SAN models are used to characterize the structural patterns. Each of these clusters has a SAN of two Au cores (a union of two Au_3, Au_4, Au_5, or Au_6 superatoms) protected by one to four

DOI: 10.1021/acs.jpcc.7b05398
J. Phys. Chem. C 2017, 121, 20458−20467

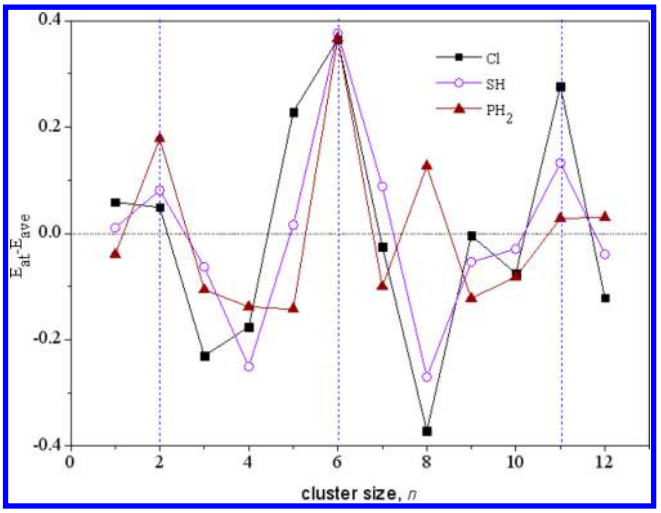

Figure 5. Plots of the energetic gaps ($E_{at} - E_{ave}$) of $Au_4(AuCl)_n$, $Au_4(AuSH)_n$, and $Au_4(AuPH_2)_n$ (n = 1−12) clusters as a function of cluster size n, where E_{at} is the atomization energy and E_{ave} is average energy. $Au_4(AuCl)_n$: $E_{ave} = 6.61522 + 4.97269n^{1/3} + 0.05075n^{2/3} - 0.0038n$. $Au_4(AuSH)_n$: $E_{ave} = 6.70115 + 4.82503n^{1/3} + 0.05833n^{2/3} - 0.00421n$. $Au_4(AuPH_2)_n$: $E_{ave} = 6.59593 + 4.81987n^{1/3} - 0.0088n^{2/3} - 1.55677 \times 10^{-4}n$.

staple motifs except $Au_4(AuPH_2)_{11}$ with a very long staple motif. The extraordinary long staple motif of $Au_4(AuPH_2)_{11}$ may be due to the weak polarity of Au−P bond. The GMs of the clusters vary from (quasi-)planar to three-dimensional as the cluster size increases. The clusters basically follow the "divide-and-protect" model and GUM. According to GUM, the Au cores of the clusters that are constructed by Au_3 and Au_4 superatoms are the elementary blocks. Ligand effects of the structures are also analyzed. For L = Cl, SH, PH_2, the clusters resemble each other when n = 1−3 and 5−7. $Au_4(AuPH_2)_8$ cluster is an interesting cluster, which is different from the corresponding $Au_4(AuCl)_8$ and $Au_4(AuSH)_8$ clusters. The structure of $Au_4(AuCl)_4$ is distinctively different from those of $Au_4(AuSH)_4$ and $Au_4(AuPH_2)_4$, probably due to the strong polarity of Au−Cl bond. The structural frameworks of $Au_4(AuL)_{1-12}$ with ligands $-SCH_3$ and −SH are identical to each other. The chemical bonding analysis is given by AdNDP method which confirms the existence of the superatoms. The aromatic properties of the superatoms have been investigated by NICS method, which indicates that the superatoms are highly aromatic. It is concluded that Au···Au aurophilic interactions weaken the aromaticity and ONs of the superatoms in some clusters. The structural evolutions of the Au cores with n in $Au_4(AuL)_n$ (L = Cl, SH, PH_2, SCH_3) clusters are presented. The size of the Au cores evolves from Au_6^{2+} to Au_7^{3+}, Au_8^{4+} and finally to Au_8^{4+}, Au_9^{5+} as n increases. This work gives a direct and overall view of size evolution of 4e-system $Au_4(AuL)_{1-12}$ (L = Cl, SH, PH_2, SCH_3) clusters in Au−L clusters, which are expected to offer some new perspectives in terms of how Au−L nanoclusters change as cluster size increases.

■ ASSOCIATED CONTENT

Supporting Information

The Supporting Information is available free of charge on the ACS Publications website at DOI: 10.1021/acs.jpcc.7b05398.

Symmetries and relative energies of the low-lying isomers of $Au_4(AuCl)_{1-12}$, $Au_4(AuSH)_{1-12}$, and $Au_4(AuPH_2)_{1-12}$ clusters, given in Figures S1−S3, respectively (PDF)

■ AUTHOR INFORMATION

Corresponding Author

*(L.C.) E-mail: clj@ustc.edu.

ORCID

Longjiu Cheng: 0000-0001-7086-6190

Author Contributions

The manuscript was written through contributions of all authors. All authors have given approval to the final version of the manuscript.

Notes

The authors declare no competing financial interest.

■ ACKNOWLEDGMENTS

This work is supported by the National Natural Science Foundation of China (21573001), by the Fuyang Teachers College (2017FSKJ01ZD), and by the Foundation of Distinguished Young Scientists of Anhui Province. The calculations were carried out at the High-Performance Computing Centre of Anhui University.

■ REFERENCES

(1) Dass, A. Mass Spectrometric Identification of $Au_{68}(SR)_{34}$ Molecular Gold Nanoclusters with 34-Electron Shell Closing. *J. Am. Chem. Soc.* **2009**, *131*, 11666−11667.

(2) Qian, H. F.; Jin, R. C. Controlling Nanoparticles with Atomic Precision: The Case of $Au_{144}(SCH_2CH_2PH)_{60}$. *Nano Lett.* **2009**, *9*, 4083−4087.

(3) Qian, H. F.; Zhu, Y.; Jin, R. C. Size-Focusing Synthesis, Optical and Electrochemical Properties of Monodisperse $Au_{38}(SC_2H_4PH)_{24}$ Nanoclusters. *ACS Nano* **2009**, *3*, 3795−3803.

(4) Heaven, M. W.; Dass, A.; White, P. S.; Holt, K. M.; Murray, R. W. Crystal Structure of the Gold Nanoparticle $[N(C_8H_{17})_4][Au_{25}(SCH_2CH_2PH)_{18}]$. *J. Am. Chem. Soc.* **2008**, *130*, 3754−3755.

(5) Zhu, M. Z.; Lanni, E.; Garg, N.; Bier, M. E.; Jin, R. C. Kinetically Controlled, High-Yield Synthesis of Au_{25} Clusters. *J. Am. Chem. Soc.* **2008**, *130*, 1138−1139.

(6) Jadzinsky, P. D.; Calero, G.; Ackerson, C. J.; Bushnell, D. A.; Kornberg, R. D. Structure of a Thiol Monolayer-Protected Gold Nanoparticle at 1.1 Resolution. *Science* **2007**, *318*, 430−433.

(7) Jung, J.; Kang, S.; Han, Y.-K. Ligand Effects on the Stability of Thiol-Stabilized Gold Nanoclusters: $Au_{25}(SR)_{18}^-$, $Au_{38}(SR)_{24}$, and $Au_{102}(SR)_{44}$. *Nanoscale* **2012**, *4*, 4206−4210.

(8) Zhu, M.; Aikens, C. M.; Hollander, F. J.; Schatz, G. C.; Jin, R. Correlating the Crystal Structure of a Thiol-Protected Au_{25} Cluster and Optical Properties. *J. Am. Chem. Soc.* **2008**, *130*, 5883−5885.

(9) Qian, H. F.; Eckenhoff, W. T.; Zhu, Y.; Pintauer, T.; Jin, R. C. Total Structure Determination of Thiolate-Protected Au_{38} Nanoparticles. *J. Am. Chem. Soc.* **2010**, *132*, 8280−8281.

(10) Zeng, C. J.; Qian, H. F.; Li, T.; Li, G.; Rosi, N. L.; Yoon, B.; Barnett, R. N.; Whetten, R. L.; Landman, U.; Jin, R. C. Total Structure and Electronic Properties of the Gold Nanocrystal $Au_{36}(SR)_{24}$. *Angew. Chem., Int. Ed.* **2012**, *51*, 13114−13118.

(11) Das, A.; Liu, C.; Zeng, C.; Li, G.; Li, T.; Rosi, N. L.; Jin, R. Cyclopentanethiolato-Protected $Au_{36}(SC_5H_9)_{24}$ Nanocluster: Crystal Structure and Implications for the Steric and Electronic Effects of Ligand. *J. Phys. Chem. A* **2014**, *118*, 8264−8269.

(12) Crasto, D.; Malola, S.; Brosofsky, G.; Dass, A.; Häkkinen, H. Single Crystal Xrd Structure and Theoretical Analysis of the Chiral $Au_{30}S(S\text{-}TBu)_{18}$ Cluster. *J. Am. Chem. Soc.* **2014**, *136*, 5000−5005.

(13) Yang, H. Y.; Wang, Y.; Edwards, A. J.; Yan, J. Z.; Zheng, N. F. High-Yield Synthesis and Crystal Structure of a Green Au_{30} Cluster

DOI: 10.1021/acs.jpcc.7b05398
J. Phys. Chem. C 2017, 121, 20458−20467

Co-Capped by Thiolate and Sulfide. *Chem. Commun.* **2014**, *50*, 14325−14327.
(14) Zeng, C. J.; Li, T.; Das, A.; Rosi, N. L.; Jin, R. C. Chiral Structure of Thiolate-Protected 28-Gold-Atom Nanocluster Determined by X-Ray Crystallography. *J. Am. Chem. Soc.* **2013**, *135*, 10011−10013.
(15) Das, A.; Li, T.; Li, G.; Nobusada, K.; Zeng, C.; Rosi, N. L.; Jin, R. C. Crystal Structure and Electronic Properties of a Thiolate-Protected Au_{24} Nanocluster. *Nanoscale* **2014**, *6*, 6458−6462.
(16) Das, A.; Li, T.; Nobusada, K.; Zeng, C.; Rosi, N. L.; Jin, R. C. Nonsuperatomic $[Au_{23}(SC_6H_{11})_{16}]^-$ Nanocluster Featuring Bipyramidal Au_{15} Kernel and Trimeric $Au_3(SR)_4$ Motif. *J. Am. Chem. Soc.* **2013**, *135*, 18264−18267.
(17) Zeng, C.; Liu, C.; Chen, Y.; Rosi, N. L.; Jin, R. C. Gold-Thiolate Ring as a Protecting Motif in the $Au_{20}(SR)_{16}$ Nanocluster and Implications. *J. Am. Chem. Soc.* **2014**, *136*, 11922−11925.
(18) Das, A.; Liu, C.; Byun, H. Y.; Nobusada, K.; Zhao, S.; Rosi, N.; Jin, R. C. Structure Determination of $[Au_{18}(SR)_{14}]$. *Angew. Chem.* **2015**, *127*, 3183−3187.
(19) Chen, S.; Wang, S. X.; Zhong, J.; Song, Y. B.; Zhang, J.; Sheng, H. T.; Pei, Y.; Zhu, M. Z. The Structure and Optical Properties of the $[Au_{18}(SR)_{14}]$ Nanocluster. *Angew. Chem., Int. Ed.* **2015**, *54*, 3145−3149.
(20) Dass, A.; Theivendran, S.; Nimmala, P. R.; Kumara, C.; Jupally, V. R.; Fortunelli, A.; Sementa, L.; Barcaro, G.; Zuo, X.; Noll, B. C. $Au_{133}(SPH\text{-}TBu)_{52}$ Nanomolecules: X-Ray Crystallography, Optical, Electrochemical, and Theoretical Analysis. *J. Am. Chem. Soc.* **2015**, *137*, 4610−4613.
(21) Chen, Y.; Zeng, C.; Liu, C.; Kirschbaum, K.; Gayathri, C.; Gil, R. R.; Rosi, N. L.; Jin, R. C. Crystal Structure of Barrel-Shaped Chiral $Au_{130}(P\text{-}Mbt)_{50}$ Nanocluster. *J. Am. Chem. Soc.* **2015**, *137*, 10076−10079.
(22) Negishi, Y.; Nobusada, K.; Tsukuda, T. Glutathione-Protected Gold Clusters Revisited: Bridging the Gap between Gold(I)-Thiolate Complexes and Thiolate-Protected Gold Nanocrystals. *J. Am. Chem. Soc.* **2005**, *127*, 5261−5270.
(23) Akola, J.; Walter, M.; Whetten, R. L.; Häkkinen, H.; Grönbeck, H. On the Structure of Thiolate-Protected Au_{25}. *J. Am. Chem. Soc.* **2008**, *130*, 3756−3757.
(24) Iwasa, T.; Nobusada, K. Theoretical Investigation of Optimized Structures of Thiolated Gold Cluster $[Au_{25}(SCH_3)_{18}]^+$. *J. Phys. Chem. C* **2007**, *111*, 45−49.
(25) Häkkinen, H.; Walter, M.; Grönbeck, H. Divide and Protect: Capping Gold Nanoclusters with Molecular Gold-Thiolate Rings. *J. Phys. Chem. B* **2006**, *110*, 9927−9931.
(26) Chaki, N. K.; Negishi, Y.; Tsunoyama, H.; Shichibu, Y.; Tsukuda, T. Ubiquitous 8 and 29 Kda Gold: Alkanethiolate Cluster Compounds: Mass-Spectrometric Determination of Molecular Formulas and Structural Implications. *J. Am. Chem. Soc.* **2008**, *130*, 8608−8610.
(27) Jiang, D. E.; Tiago, M. L.; Luo, W. D.; Dai, S. The "Staple" Motif: A Key to Stability of Thiolate-Protected Gold Nanoclusters. *J. Am. Chem. Soc.* **2008**, *130*, 2777−2779.
(28) Jiang, D. E.; Luo, W. D.; Tiago, M. L.; Dai, S. In Search of a Structural Model for a Thiolate-Protected Au_{38} Cluster. *J. Phys. Chem. C* **2008**, *112*, 13905−13910.
(29) Pei, Y.; Gao, Y.; Zeng, X. C. Structural Prediction of Thiolate-Protected Au_{38}: A Face-Fused Bi-Icosahedral Au Core. *J. Am. Chem. Soc.* **2008**, *130*, 7830−7832.
(30) Lopez Acevedo, O.; Tsunoyama, H.; Tsukuda, T.; Aikens, C. M.; et al. Chirality and Electronic Structure of the Thiolate-Protected Au_{38} Nanocluster. *J. Am. Chem. Soc.* **2010**, *132*, 8210−8218.
(31) Jiang, D. E.; Overbury, S. H.; Dai, S. Structure of $Au_{15}(SR)_{13}$ and Its Implication for the Origin of the Nucleus in Thiolated Gold Nanoclusters. *J. Am. Chem. Soc.* **2013**, *135*, 8786−8789.
(32) Nimmala, P. R.; Knoppe, S.; Jupally, V. R.; Delcamp, J. H.; Aikens, C. M.; Dass, A. $Au_{36}(SPH)_{24}$ Nanomolecules: X-Ray Crystal Structure, Optical Spectroscopy, Electrochemistry, and Theoretical Analysis. *J. Phys. Chem. B* **2014**, *118*, 14157−14167.
(33) Walter, M.; Moseler, M.; Whetten, R. L.; Häkkinen, H. A 58-Electron Superatom-Complex Model for the Magic Phosphine-Protected Gold Clusters of 1.4-nm Dimension. *Chem. Sci.* **2011**, *2*, 1583−1587.
(34) Akola, J.; Walter, M.; Whetten, R. L.; Häkkinen, H.; Grönbeck, H. On the Structure of Thiolate-Protected Au_{25}. *J. Am. Chem. Soc.* **2008**, *130*, 3756−3757.
(35) Walter, M.; Akola, J.; Lopez Acevedo, O.; Jadzinsky, P. D.; Calero, G.; Ackerson, C. J.; Whetten, R. L.; Grönbeck, H.; Häkkinen, H. A Unified View of Ligand-Protected Gold Clusters as Superatom Complexes. *Proc. Natl. Acad. Sci. U. S. A.* **2008**, *105*, 9157−9162.
(36) Jiang, D. E.; Chen, W.; Whetten, R. L.; Chen, Z. F. What Protects the Core When the Thiolated Au Cluster Is Extremely Small? *J. Phys. Chem. C* **2009**, *113*, 16983−16987.
(37) Jiang, D. E.; Whetten, R. L.; Luo, W. D.; Dai, S. The Smallest Thiolated Gold Superatom Complexes. *J. Phys. Chem. C* **2009**, *113*, 17291−17295.
(38) Jiang, D. E.; Walter, M.; Akola, J. On the Structure of a Thiolated Gold Cluster: $Au_{44}(SR)_{28}^{2-}$. *J. Phys. Chem. C* **2010**, *114*, 15883−15889.
(39) Gao, Y.; Shao, N.; Zeng, X. C. Ab Initio Study of Thiolate-Protected Au_{102} Nanocluster. *ACS Nano* **2008**, *2*, 1497−1503.
(40) Gao, Y. Ligand Effects of Thiolate-Protected Au_{102} Nanoclusters. *J. Phys. Chem. C* **2013**, *117*, 8983−8988.
(41) Cheng, L. J.; Yuan, Y.; Zhang, X. Z.; Yang, J. L. Superatom Networks in Thiolate-Protected Gold Nanoparticles. *Angew. Chem., Int. Ed.* **2013**, *52*, 9035−9039.
(42) Tian, Z. M.; Cheng, L. J. Perspectives on the Energy Landscape of Au-Cl Binary Systems from the Structural Phase Diagram of Au_xCl_y ($x + y = 20$). *Phys. Chem. Chem. Phys.* **2015**, *17*, 13421−13428.
(43) Lopez Acevedo, O.; Akola, J.; Whetten, R. L.; Gronbeck, H.; Häkkinen, H. Structure and Bonding in the Ubiquitous Icosahedral Metallic Gold Cluster $Au_{144}(SR)_{60}$. *J. Phys. Chem. C* **2009**, *113*, 5035−5038.
(44) Knoppe, S.; Wong, O. A.; Malola, S.; Häkkinen, H.; Bürgi, T.; Verbiest, T.; Ackerson, C. J. Chiral Phase Transfer and Enantioenrichment of Thiolate-Protected Au102 Clusters. *J. Am. Chem. Soc.* **2014**, *136*, 4129−4132.
(45) Xu, W. W.; Gao, Y.; Zeng, X. C. Unraveling Structures of Protection Ligands on Gold Nanoparticle $Au_{68}(SH)_{32}$. *Sci. Adv.* **2015**, *1*, e1400211.
(46) Xu, W. W.; Zhu, B. E.; Zeng, X. C.; Gao, Y. A Grand Unified Model for Liganded Gold Clusters. *Nat. Commun.* **2016**, *7*, 13574.
(47) Liu, W. D.; Cheng, L. J. Size Evolution of 2e-Superatom in Ligand-Protected Au Nanoclusters: Au_2-$(AuL)_{1-12}$ (L = Cl, SH, SCH_3, PH_2 and $P(CH_3)_2$). *J. Phys. Chem. C* **2016**, *120*, 2432−2438.
(48) Ren, L.; Cheng, L. J.; Feng, Y.; Wang, X. M. Geometric and Electronic Structures of $(BeO)_n$ (n = 2−12, 16, 20, and 24): Rings, Double Rings, and Cages. *J. Chem. Phys.* **2012**, *137*, 014309.
(49) Cheng, L. J. B_{14}: An All-Boron Fullerene. *J. Chem. Phys.* **2012**, *136*, 104301.
(50) Cheng, L. J.; Yang, J. L. Communication: New Insight into Electronic Shells of Metal Clusters: Analogues of Simple Molecules. *J. Chem. Phys.* **2013**, *138*, 141101.
(51) Li, L. F.; Cheng, L. J. First Principle Structural Determination of $(B_2O_3)_n$ (n = 1−6) Clusters: From Planar to Cage. *J. Chem. Phys.* **2013**, *138*, 094312.
(52) Yuan, Y.; Cheng, L. J. B_{14}^{2+}: A Magic Number Double-Ring Cluster. *J. Chem. Phys.* **2012**, *137*, 044308.
(53) Alexandrova, A. N.; Boldyrev, A. I.; Fu, Y. J.; Yang, X.; Wang, X. B.; Wang, L. S. Structure of the Na_xCl_{x+1} (x = 1−4) $Na_xCl_{x+1}^-$ (x = 1−4) Clusters via ab initio Genetic Algorithm and Photoelectron Spectroscopy. *J. Chem. Phys.* **2004**, *121*, 5709−5719.
(54) Alexandrova, A. N.; Boldyrev, A. I. Search for the $Li_n^{0/+1/-1}$ (n = 5 7) Lowest-Energy Structures Using the ab Initio Gradient Embedded Genetic Algorithm (GEGA). Elucidation of the Chemical Bonding in the Lithium Clusters. *J. Chem. Theory Comput.* **2005**, *1*, 566−580.

DOI: 10.1021/acs.jpcc.7b05398
J. Phys. Chem. C 2017, 121, 20458−20467

(55) Deaven, D. M.; Ho, K. M. Molecular Geometry Optimization with a Genetic Algorithm. *Phys. Rev. Lett.* **1995**, *75*, 288−291.
(56) Johnston, R. L. Evolving Better Nanoparticles: Genetic Algorithms for Optimising Cluster Geometries. *Dalton Trans.* **2003**, 4193−4207.
(57) Shayeghi, A.; Götz, D.; Davis, J.; Schaefer, R.; Johnston, R. L. Pool-Bcga: A Parallelised Generation-Free Genetic Algorithm for the Ab Initio Global Optimisation of Nanoalloy Clusters. *Phys. Chem. Chem. Phys.* **2015**, *17*, 2104−2112.
(58) Frisch, M.; Trucks, G.; Schlegel, H. B.; Scuseria, G.; Robb, M.; Cheeseman, J.; Scalmani, G.; Barone, V.; Mennucci, B.; Petersson, G., et al. *Gaussian 09*, Revision A. 02; Gaussian. Inc.: Wallingford, CT, 2009.
(59) Schuchardt, K. L.; Didier, B. T.; Elsethagen, T.; Sun, L.; Gurumoorthi, V.; Chase, J.; Li, J.; Windus, T. L. Basis Set Exchange: A Community Database for Computational Sciences. *J. Chem. Inf. Model.* **2007**, *47*, 1045−1052.
(60) Weigend, F.; Ahlrichs, R. Balanced Basis Sets of Split Valence, Triple Zeta Valence and Quadruple Zeta Valence Quality for H to Rn: Design and Assessment of Accuracy. *Phys. Chem. Chem. Phys.* **2005**, *7*, 3297−3305.
(61) Tao, J.; Perdew, J. P.; Staroverov, V. N.; Scuseria, G. E. Climbing the Density Functional Ladder: Nonempirical Meta-Generalized Gradient Approximation Designed for Molecules and Solids. *Phys. Rev. Lett.* **2003**, *91*, 146401.
(62) Glendening, E. D.; Badenhoop, J. K.; Reed, A. E.; Carpenter, J. E.; Bohmann, J. A.; Morales, C. M.; Weinhold, F. *Nbo 5.0*;. Theoretical Chemistry Institute, University of Wisconsin: Madison, WI, 2001.
(63) Zubarev, D. Y.; Boldyrev, A. I. Developing Paradigms of Chemical Bonding: Adaptive Natural Density Partitioning. *Phys. Chem. Chem. Phys.* **2008**, *10*, 5207−5217.
(64) Sergeeva, A. P.; Averkiev, B. B.; Zhai, H. J.; Boldyrev, A. I.; Wang, L. S. All-Boron Analogues of Aromatic Hydrocarbons: B_{17}^- and B_{18}^-. *J. Chem. Phys.* **2011**, *134*, 224304.
(65) Huang, W.; Sergeeva, A. P.; Zhai, H. J.; Averkiev, B. B.; Wang, L. S.; Boldyrev, A. I. A Concentric Planar Doubly Π-Aromatic B_{19}^- Cluster. *Nat. Chem.* **2010**, *2*, 202.
(66) Cheng, L. J.; Zhang, X. Z.; Jin, B. K.; Yang, J. L. Superatom-Atom Super-Bonding in Metallic Clusters: A New Look to the Mystery of an Au_{20} Pyramid. *Nanoscale* **2014**, *6*, 12440−12444.
(67) Zubarev, D. Y.; Boldyrev, A. I. Deciphering Chemical Bonding in Golden Cages. *J. Phys. Chem. A* **2009**, *113*, 866−868.
(68) Cheng, L. J.; Ren, C. D.; Zhang, X. Z.; Yang, J. L. New Insight into the Electronic Shell of $Au_{38}(SR)_{24}$: A Superatomic Molecule. *Nanoscale* **2013**, *5*, 1475−1478.
(69) Pei, Y.; Lin, S. S.; Su, J. C.; Liu, C. Y. Structure Prediction of $Au_{44}(SR)_{28}$: A Chiral Superatom Cluster. *J. Am. Chem. Soc.* **2013**, *135*, 19060−19063.
(70) Varetto, U. *Molekel*, Version 5.4. 0.8; Swiss National Supercomputing Centre: Manno, Switzerland, 2009.
(71) Sergeeva, A. P.; Boldyrev, A. I. Rational Design of Small 3D Gold Clusters. *J. Cluster Sci.* **2011**, *22*, 321−329.
(72) Jiang, D. E.; Walter, M. The Halogen Analogs of Thiolated Gold Nanoclusters. *Nanoscale* **2012**, *4*, 4234−4239.
(73) Yu, Y.; Luo, Z. T.; Chevrier, D. M.; Leong, D. T.; Zhang, P.; Jiang, D. E.; Xie, J. P. Identification of a Highly Luminescent $Au_{22}(SG)_{18}$ Nanocluster. *J. Am. Chem. Soc.* **2014**, *136*, 1246−1249.
(74) Pei, Y.; Pal, R.; Liu, C.; Gao, Y.; Zhang, Z.; Zeng, X. C. Interlocked Catenane-Like Structure Predicted in $Au_{24}(SR)_{20}$: Implication to Structural Evolution of Thiolated Gold Clusters from Homoleptic Gold(I) Thiolates to Core-Stacked Nanoparticles. *J. Am. Chem. Soc.* **2012**, *134*, 3015−3024.
(75) Yang, S.; Chai, J. S.; Song, Y. B.; Kang, X.; Sheng, H. T.; Chong, H. B.; Zhu, M. Z. A New Crystal Structure of Au_{36} with a Au_{14} Kernel Cocapped by Thiolate and Chloride. *J. Am. Chem. Soc.* **2015**, *137*, 10033−10035.
(76) Gutrath, B. S.; Oppel, I. M.; Presly, O.; Beljakov, I.; Meded, V.; Wenzel, W.; Simon, U. $[Au_{14}(PPh_3)_8(NO_3)_4]$: An Example of a New Class of $Au(NO_3)$-Ligated Superatom Complexes. *Angew. Chem., Int. Ed.* **2013**, *52*, 3529−3532.
(77) Shichibu, Y.; Negishi, Y.; Watanabe, T.; Chaki, N. K.; Kawaguchi, H.; Tsukuda, T. Biicosahedral Gold Clusters $[Au_{25}(PPh_3)_{10}(SC_nH_{2n+1})_5Cl_2]_2$ (n = 2−18): A Stepping Stone to Cluster-Assembled Materials. *J. Phys. Chem. C* **2007**, *111*, 7845−7847.
(78) Stefanescu, D. M.; Yuen, H. F.; Glueck, D. S.; Golen, J. A.; Rheingold, A. L. Synthesis and Structure of Cyclic Gold(I) Phosphanyl Complexes $[\{Au(PR_2)\}_n]$. *Angew. Chem., Int. Ed.* **2003**, *42*, 1046−1048.
(79) Stefanescu, D. M.; Yuen, H. F.; Glueck, D. S.; Golen, J. A.; Zakharov, L. N.; Incarvito, C. D.; Rheingold, A. L. Gold(I) Phosphido Complexes: Synthesis, Structure, and Reactivity. *Inorg. Chem.* **2003**, *42*, 8891−8901.
(80) Stefanescu, D. M.; Glueck, D. S.; Siegel, R.; Wasylishen, R. E. Synthesis and Characterization of Phosphido-Monolayer-Protected Gold Nanoclusters. *Langmuir* **2004**, *20*, 10379−10381.
(81) Lane, E. M.; Chapp, T. W.; Hughes, R. P.; Glueck, D. S.; Feland, B. C.; Bernard, G. M.; Wasylishen, R. E.; Rheingold, A. L. Synthesis of Gold Phosphido Complexes Derived from Bis(secondary) Phosphines. Structure of Tetrameric $[Au(MesP(CH_2)_3PMes)Au]_4$. *Inorg. Chem.* **2010**, *49*, 3950−3957.
(82) Liu, Y.; Tian, Z. M.; Cheng, L. J. Size Evolution and Ligand Effects on the Structures and Stability of $(AuL)_n$ (L = Cl, SH, SCH_3, PH_2, $P(CH_3)_2$, n = 1−13) Clusters. *RSC Adv.* **2016**, *6*, 4705−4712.
(83) Schleyer, P. v. R.; Maerker, C.; Dransfeld, A.; Jiao, H. J.; Hommes, N. J. v. E. Nucleus-Independent Chemical Shifts: A Simple and Efficient Aromaticity Probe. *J. Am. Chem. Soc.* **1996**, *118*, 6317−6318.
(84) Chen, Z. F.; King, R. B. Spherical Aromaticity: Recent Work on Fullerenes, Polyhedral Boranes, and Related Structures. *Chem. Rev.* **2005**, *105*, 3613−3642.
(85) Boldyrev, A. I.; Wang, L. S. All-Metal Aromaticity and Antiaromaticity. *Chem. Rev.* **2005**, *105*, 3716−3757.
(86) Li, X.; Kuznetsov, A. E.; Zhang, H. F.; Boldyrev, A. I.; Wang, L. S. Observation of All-Metal Aromatic Molecules. *Science* **2001**, *291*, 859−861.
(87) Jiménez Halla, J. O. C.; Matito, E.; Robles, J.; Solà, M. Nucleus-Independent Chemical Shift (NiCS) Profiles in a Series of Monocyclic Planar Inorganic Compounds. *J. Organomet. Chem.* **2006**, *691*, 4359−4366.
(88) Cheeseman, J. R.; Trucks, G. W.; Keith, T. A.; Frisch, M. J. A Comparison of Models for Calculating Nuclear Magnetic Resonance Shielding Tensors. *J. Chem. Phys.* **1996**, *104*, 5497.

DOI: 10.1021/acs.jpcc.7b05398
J. Phys. Chem. C 2017, 121, 20458−20467